The impact of metabolism on aging and cell size in single yeast cells

Huberts, Daphne

Link to publication in University of Groningen/UMCG research database

Chapter 5

Post-mitotic protein production causes cell size to increase with replicative age in *Saccharomyces cerevisiae*

Daphne H E W Huberts, Christoffer Åberg, Athanasios Litsios, Gesa Behrends & Matthias Heinemann

Abstract

While an increased cell size is a hallmark of aged *S. cerevisiae*, it is unclear how cells grow in size with replicative age. Using a microfluidic device for long-term microscopic monitoring of replicating yeast, we found a linear increase in cell size with replicative age. A model-based analysis of protein synthesis data shows that the rate of protein synthesis surpassed the rate of protein transfer to the bud after mitosis, leading to protein accumulation and cell size growth in the mother cell. Consecutive rounds of cell division and the accompanying periods of protein overproduction result in a linear increase in cell volume with replicative age. The magnitude of the imbalance between protein production and protein transfer to the bud can be modulated using different carbon sources causing the cell to grow in size at different rates with replicative age. We hypothesize that post-mitotic protein production is a necessity for mother cells to enter the next round of cell division, rendering cell size increase with replicative age a consequence of reproduction.

Introduction

In yeast and several types of mammalian cells, an increased cell size is a hallmark of aging (1, 2). Increased cell size may have important consequences for cellular function (3). For instance, a reduced surface-to-volume ratio may result in lower amounts of nutrients being imported per cell volume and time. Such a reduction in the carbon uptake rate could be responsible for the observed switch from fermentation to a more respiratory mode of metabolism with age (4-6). In addition, an increased cell size may cause senescence (1, 7, 8). For example, the replicative lifespan and the volume of a cell at the start of its first cell division were found to correlate (1, 9). Mutants with a reduced cell size have an increased replicative lifespan, while cells with a larger cell volume have a shortened replicative lifespan (1). Also, cells were found to die at a relatively constant cell size. Yet, there is evidence that does not support the notion that cell size causes senescence (9, 10). Deletion of fob1 increases RLS without altering cell size (11) and diploid yeast cells, which are larger than haploid yeast cells, have longer replicative lifespans than their haploid counterparts (12) showing that there is not necessarily a link between RLS and cell size. Furthermore, cells were observed to stop dividing at a range of sizes (10).

Although changes in cell size during aging appear to be well documented (13), the characteristics of the cell size increase with replicative age in *S. cerevisiae* are unclear. Several groups found evidence that suggest that cells grow in size exponentially (14-16), while others showed that cell size increases in a linear manner (1). Moreover, it remains essentially unknown why cells increase in cell size with age (7, 9).

Here, using a microfluidic device for long-term microscopic observation of yeast cells (17), we investigated the dynamics of cell size increase with replicative age. By collecting cell size and protein synthesis data and integrating this data in a differential equation model, we unraveled the dynamic rates of protein production and transfer to the bud throughout the cell cycle. We found that the protein synthesis rate does not drop fast enough after mitosis leading to a period of protein overproduction during each round of cell division. This lack of homeostasis during cell division leads to a constant cell size increase rate with replicative age. We therefore conclude that the increase in cell size with replicative age appears to be a consequence of cell division.

Materials and methods

Strains and strain construction

All experiments were performed with the S288c-derived YSBN6 [MATa FY3 ho::HphMX4] (18). YSBN6 Whi5-GFP::HIS was obtained from Mareike Schmidt (ETH Zürich, Zürich, Switzerland). YSBN6 ptetO7-mCherry-sfGFP::KanMX was constructed by combining fragments from three different plasmids by Gibson assembly (Gibson Assembly® Cloning Kit, E5510S, New England Biolabs). A 1.5 kb PCR fragment containing the fluorescent protein timer (19) was ob-

tained from vector pMAM17 (pFA6a-mCherry-sfGFP-kanMX obtained from Michael Knop, Center for Molecular Biology of the University of Heidelberg (ZMBH), Heidelberg, Germany) and primers TET-GFP.fw (5'-CACAAATACA-CACACTAAATTACCGGAT   CAATTCGGGATGGTGAGCAAGGGCGAGG-3') and TET-GFP.rw (5'-CGTGACATAACTAATTACATGATGCGGCCCTCTTAG-GATCCCTTATAAAGCTCGTCCATTCC-3'). In parallel, an 8 kb fragment containing the tetracycline repressible promoter (ptetO7) was generated from the vector pCM189 (ATCC 87661) containing the ptetO7 using primers PCM189-Tet.fw (5'-GAGGGCCGCATCATGTAATTAGTTATGT-3') and PCM189-Tet.rv (5'-CCCGATTGATCCGGTAATTTAGTGTGT-3'). Both PCR fragments were assembled using Gibson assembly to generate pMAM17-mCherry-sfGFP. The newly generated plasmid was subsequently used to generate a 4.3 kb fragment containing ptetO7-mCherry-sfGFP using primers T-PCM189.fw01 (5'-GAGG-GCCGCATCATGTAATTAG-3') and P-PCM189.rv01 (5'-CCCGAATTGATCCG-GTAATTTAG-3'), while a 6 kb fragment with the HO integration regions and KanMX selectable marker was produced from the vector HO-poly-KanMX4-HO (ATCC 87804) using the primers TET-HO#1.fw (5'- CTACCCACCGTACTCGT-CAATTCCGGCCAGCGACAT GGAGGCC-3') and TET-HO#1.rv (5'- AAGCTTG-GCCGCAAATTAAAGCCCGTACGCCATTTT AAGTCCAAAG-3'). The final plasmid HO-ptetO7-mCherry-sfGFP-KanMX-HO was then generated using Gibson assembly from the fragments ptetO7-mCherry-sfGFP and HO-KANMX-HO. Using primers HO#1-fw (5'-TCAAGGAGAGAGAACTACCACT-3') and HO#1-rv (5'-TGCCCAATTTTTCGCCTTTGT-3') the complete fragment containing HO-ptetO7-mCherry-sfGFP-KanMX-HO was produced. The fragment HO-ptetO7-mCherry-sfGFP-KanMX-HO was then transformed into YSBN6 using the Gietz Long Protocol (20). Subsequent selection of transformants for resistance to geneticin (G418) was carried out by plating cells on YPD plates containing 200µg/mL G418. Integration of HO-ptetO7-mCherry-sfGFP-KanMX-HO was further confirmed by the presence of red and green fluorescence in the transformants.

Media and cultivation

YPD plates were prepared by adding 20 g/L agar to complete rich medium (50 g/L YPD; Formedium). For liquid cultures minimal medium (6.9 g/L yeast nitrogen base (YNB); Formedium) was supplemented with filter-sterilized 20 g/L glucose (2% (wt/vol) D-glucose monohydrate; Sigma), 20 g/L galactose (2% (wt/vol) D-galactose; Sigma) or 20 g/L sodium pyruvate (2% (wt/vol) sodium pyruvate; Sigma). One day before the experiment, cells were taken from the -80 °C freezer, streaked on YPD plates, and incubated overnight at 30 °C. A single colony was used to inoculate a 100-mL flask containing 10 mL YNB medium with 2% (wt/vol) glucose, galactose or pyruvate. The flask was then incubated overnight at 30 °C with shaking at 300 rpm (Climo-Shaker ISF1-x, Kühner AG, Switzerland). For glucose and galactose, the culture was diluted the next morning into a new 100 mL flask containing 10 mL medium with 2% (wt/vol) glucose or galactose to yield an OD_{600nm} of 0.3 after roughly 8 h. The culture was then diluted again and incubated overnight to yield an OD_{600nm} of about 0.3 the next morning at the start

of the aging experiment or cell size measurement. For 2% (wt/vol) pyruvate, the flask was incubated overnight at 30 °C for 36 h after inoculation. Thereafter, the culture was diluted into a new 100 mL flask containing 10 mL YNB medium with 2% (wt/vol) pyruvate and grown to an OD_{600nm} of 0.3 after 24 h. The culture was then diluted and allowed to grow to OD_{600nm} 0.3 in another 24 h before performing an experiment. This preculture procedure ensured that the cells were growing exponentially at the start of all experiments.

Microscopy and microfluidic dissection platform

All microscopy experiments were performed using a microfluidic dissection platform (21, 22) in combination with an inverted fluorescence microscope (Eclipse Ti-E; Nikon Instruments). The microscope was housed in an incubator (Life Imaging Services) for cultivation at 30 °C. Unless specified otherwise, images were taken every 10 min using a 60x objective (CFI Plan Apo; Nikon; NA = 1.4; working distance = 0.13 mm) and an iXon Ultra 897 camera (Andor) with a 1 MHz readout speed. For brightfield imaging, a UV blocking filter was used. Fluorescence experiments were performed using LED-based illumination (pE2; CoolLed; 470 nm for GFP and 565 nm for mCherry) in combination with appropriate filters (for GFP; 470/40 nm excitation, 525/50 nm emission and for mCherry; 560/40 nm excitation, 625/40 nm emission). For GFP measurements of YSBN6 Whi5-GFP::HIS, cells were exposed for 100 ms at 470 nm with 10% light intensity (pE2; CoolLed) using 2x2 binning and an EM gain of 75. Images were taken every 5 minutes for cells growing on glucose and captured using a readout speed of 80 kHz. For fluorescence measurements of YSBN6 ptetO7-mCherry-sf-GFP::KanMX, cells were exposed for 100 ms at 525 nm with 20% light intensity to measure mCherry fluorescence intensity, followed by exposure for 100 ms at 470 nm with 10 % light intensity to measure sfGFP fluorescence intensity. Microscope images were captured using an EM gain of 50 for mCherry and of 25 for sfGFP.

Image analysis

Cytokinesis, which was marked by a darkening of the bud neck (23) and initiation of cell division marked by the appearance of a bud were determined by visual inspection of brightfield images. The cells' growth rate in the microfluidic device was determined from the time in hours between the appearances of two subsequent buds, referred to as division time. Whi5-GFP localization was denoted as nuclear when GFP fluorescence appeared as a single bright spot within the cell, and as cytoplasmic in the absence of such a fluorescent spot. Cell sizes and fluorescence intensities were determined with the BudJ plugin for ImageJ (24). Cellular fluorescence intensity was corrected for background signal using the modal gray value of each image. To correct fluorescence for unevenness in the illumination across the field of view, we determined the fluorescence intensity of more than 300 cells as a function of the x- and y-coordinates of the field of view. Here we found that there was linear dependency on x- and y-coordinate of the

field of view and the fluorescence intensity. We then generated linear functions to describe the dependency of the fluorescence intensity on the x- or y-coordinate with which we corrected the original image to obtain the flat-field image (25).

Differential equation model

To determine the dynamic production and transfer rates, a differential equation model was developed that described the dynamic changes in the number of mCherry-sfGFP fusion proteins in the mother and daughter cell, distinguishing between matured and non-matured versions. In addition to the maturation kinetics of mCherry and sfGFP (19) and a constant protein degradation rate, the model included a dynamic protein production rate for both mother as well as daughter cells and a dynamic protein transfer rate from mother to daughter. Measured mCherry and sfGFP fluorescence intensities were used to determine the numbers of fluorescent protein timers with and without matured mCherry. We corrected for a reduction in the brightness of sfGFP in the presence of mature mCherry due to Förster Resonance Energy Transfer (FRET) using a previously determined FRET factor (19). The dynamic rates of protein production, transfer and constant rate of degradation were then determined by least-square fitting of the model to the dynamic data that included mCherry and sfGFP fluorescence intensities and cell volumes. For the fitting, the experimental data was divided into three datasets depending on the duration between bud appearance and cytokinesis (50, 60 or 70 min with n = 32 to 83 cells per data set). A detailed description of the model can be found in the Supplementary Information.

Results

Cell size increases linearly with replicative age.

To understand why cells grow in size with replicative age, we first investigated how cell size develops with replicative age. For this purpose, we used our microfluidic dissection platform (21) and continuously measured the size of single cells on different carbon sources for up to five days. Here, we observed large increases in cell volume with age. For instance, on glucose, the cell volume increased up to 4-fold from roughly 60 fL to 250 fL. On all three tested carbon sources, we found a linear increase in cell volume with replicative age (Figure 1A; Spearman's rho test; correlation coefficient of 0.95 on glucose, 0.93 on galactose and 0.89 on pyruvate; P < 0.001 for all tested carbon sources). Linearity of the cell size increase was demonstrated by the fact that residuals after the linear regression scattered in an even manner along the replicative age (Figure S1). A linear increase in cell volume with replicative age means that cell size increases with a constant volume increment in each cell division irrespective of the current volume or replicative age of the cell.
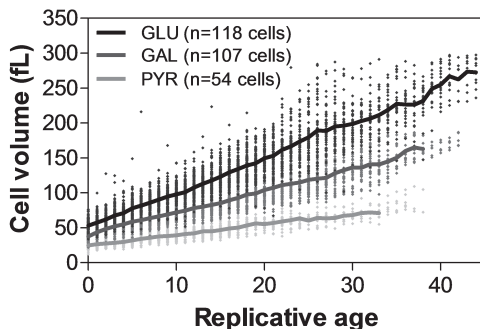
Figure 1. Cell volume increases linearly with replicative age. The average cell volume per carbon source is shown with a line. Outliers were removed from each data set by fitting a linear trend line through all of the data points for each carbon source ($R^2 = 0.996$ for glucose, $R^2 = 0.996$ for galactose and $R^2 = 0.992$) and deleting data points with the greatest residuals in an iterative fashion until 1% of the original number of data points per carbon source was deleted. From the linear regressions, we determined a cell volume increase per cell division of 5.0 ± 0.5 fL/bud on glucose, 3.2 ± 0.3 fL/bud on galactose and 1.5 ± 0.02 fL// bud on pyruvate. Cells were not necessarily tracked until cell death.

Cell volume oscillates during the cell cycle

To investigate the cause for the constant, but condition-dependent, cell volume increase with each cell division, we zoomed into single cell division cycles and asked whether the cell size increase is constant throughout the cell cycle or whether the increase is confined to a specific cell cycle phase. Therefore, we measured the cell size of individual cells every two minutes during cell division cycles. Here, we found that the size of the mother cell oscillates during each cell cycle (Figure 2A & B). The size of the mother cell slightly decreases during the first half of the cell cycle after bud appearance (Figure 2C & D; 1.8 ± 0.2 fL ($\pm$ SEM) on glucose; 1.0 ± 0.3 ($\pm$ SEM) fL on pyruvate), but strongly increases in the second half of the cell cycle until appearance of the next bud (Figure 2C & D; 5.8 ± 0.2 ($\pm$ SEM) fL on glucose; 2.8 ± 0.4 ($\pm$ SEM) fL on pyruvate). As the increase in cell size during the second half of the cell cycle is larger than the decrease during the first half of the cell cycle, the size of the mother cell grows with every round of cell division and thus with replicative age (Figure 1).

Cell volume increases after Whi5 localizes to the nucleus

Next, we asked what triggered the increase in cell size during each round of cell cycle division. We hypothesized that the cell size increase coincided with the physical separation of the daughter cell from the mother cell, termed cytokinesis (26). We therefore determined the onset of cytokinesis in brightfield images by looking for a characteristic darkening of the bud neck (23). Here, we found that cell size started to increase prior to cytokinesis (Figure 3A) suggesting that cytokinesis most likely does not trigger the increase in cell size. We therefore focused
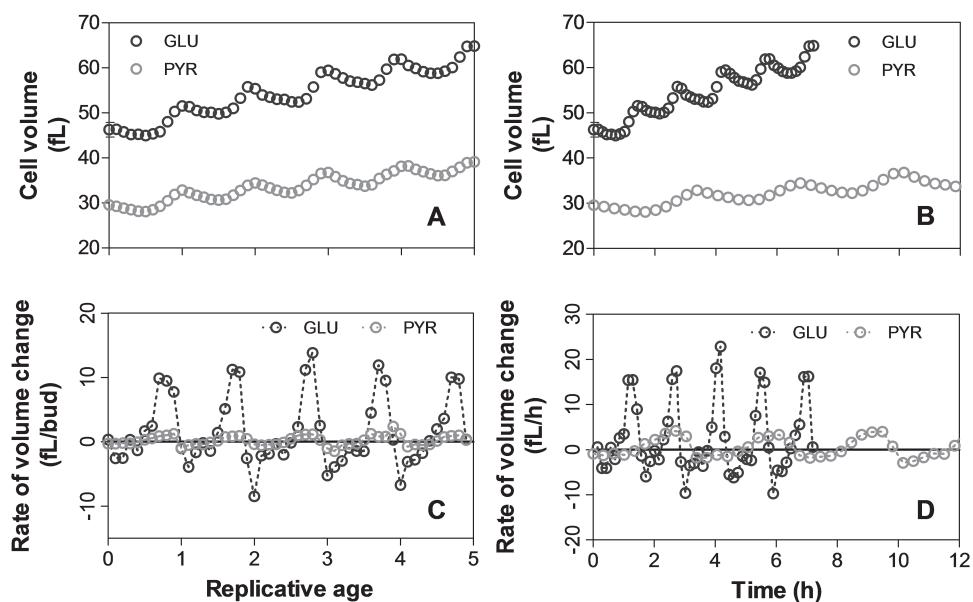
Figure 2. Cell volume of the mother cell oscillates during the cell cycle. Cell volume was plotted versus replicative age (A) and versus time in hours (B). The rate of cell volume change between subsequent data points was plotted as a function of replicative age (C) or time (D). Bud appearance marked the start of cell division and cells had a replicative age of 0 when the first bud appeared. For glucose (black), at least 430 cell volume measurements were averaged per data point, while for pyruvate (grey) n≥526 measurements were averaged per data point. The maximum SEM was 1.6 fL on glucose and 0.3 fL on pyruvate.

on the cell cycle event preceding cytokinesis, which is mitosis, using the dynamic localization changes of GFP-tagged Whi5. Whi5 is a cell cycle regulated repressor of G1/S transcription (27, 28), which enters the nucleus at the end of mitosis and leaves the nucleus at START, when the cell commits itself to a new round of cell division. When we determined the Whi5-GFP localization as function of the cell cycle progression, we found that the onset of cell size growth in mother cells coincides with transfer of Whi5 to the nucleus, both on glucose (Figure 3B) as well as on pyruvate (Figure S2). Thus, mother cells increase in size after mitotic exit and continue to do so during G1.

Post-mitotic protein production causes cell size to increase

As mother cells increase in cell size after mitotic exit, we asked whether the changes in cell size could reflect biomass production not slowing down or not slowing down rapidly enough after mitotic exit. Therefore, we estimated the dynamically changing rates of protein synthesis in mother and daughter cells and the rate of protein transfer between mother and daughter cells during the cell
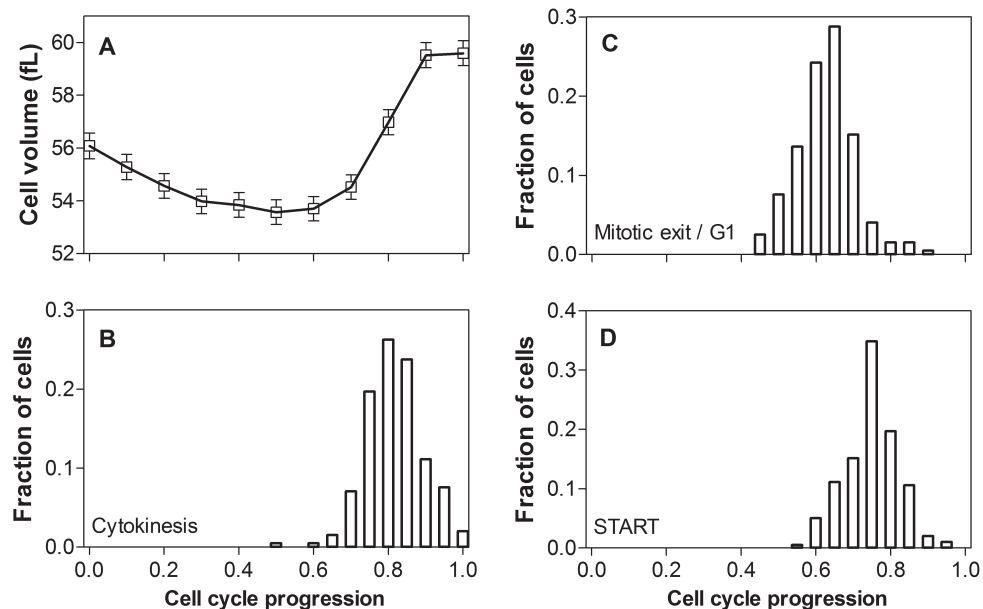
Figure 3. Cell volume increase in mother cells coincides with mitotic exit. Cell cycle duration was normalized using the time between subsequent budding events and defining the time point prior to bud appearance as t = 0. Dotted lines indicate the 95% confidence intervals of the mean. Cells were grown on glucose. (A) Cell volume as a function of cell cycle progression. (B) Histogram representing the distribution of cell cycle progression at which cytokinesis occurred (t = 0.8 ± 0.01 (± SEM)); n = 198 cell divisions. Cell volume starts to increase around t = 0.7, when cytokinesis has only occurred in a minority of the cells suggesting that cytokinesis does not coincide with an increase in cell volume. (C&D) Histogram representing the distribution of cell cycle progression at which Whi5-GFP enters the nucleus referred to as mitotic exit/G1 (C) or exits the nucleus referred to as START (D). On average, Whi5 enters the nucleus at t = 0.6 (SEM < 0.01; n = 198 cell divisions) and exits again at t = 0.73 (SEM < 0.01; n = 198 cell divisions) of cell cycle progression. The cell volume starts to increase at the same time as Whi5 enters the nucleus and continues after Whi5-GFP exits again from the nucleus.

division cycle. For this purpose, we expressed a fusion protein of mCherry and superfolding GFP (sfGFP) referred to as the tandem fluorescent 'protein timer' developed by Khmelinskii *et al.* (2012) (19). Because sfGFP has a maturation time of several minutes and the red mCherry protein matures with a half-time of roughly 40 minutes (19), the ratio between red and green fluorescence contains information about when the fusion protein was produced. To estimate the dynamic protein production and transfer rates, we measured cell volume and mCherry and sfGFP fluorescence intensity during cell division (Fig S3).

Because the time between bud appearance and cytokinesis varied among individual cells, we grouped the single cell data, *i.e.* dynamic fluorescence intensities and cell volume data, into categories depending on the time between bud

appearance and cytokinesis and only used the most populated categories (50, 60 or 70 min) for further analysis. The experimental data of each of these categories was then individually fitted to a differential equation model (cf. Supplementary Information; Figure S4) to determine the time-dependent rates of protein production in mother (Figure 4A) and daughter (Figure 4B), the dynamic protein transfer rate between mother and daughter (Figure 4C), and the protein degradation rate.

Here, we found that after appearance of the bud (t = 0), the protein production rate of the mother cell, which is expressed as GFP fluorescence intensity produced per minute, increased until halfway through the cell cycle (Figure 4A). The rate of protein transfer to the daughter cell increased after bud appearance
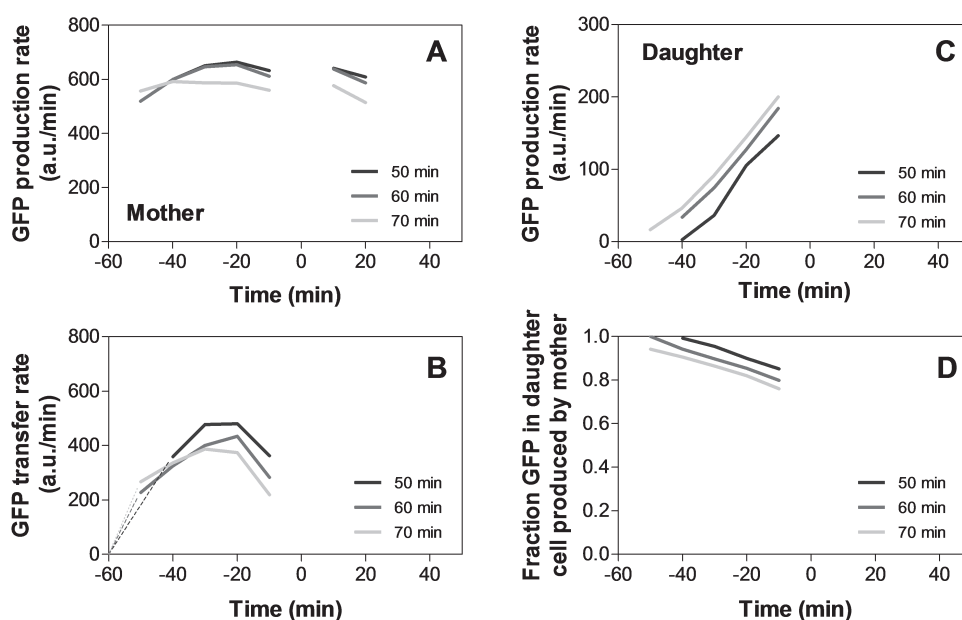

Figure 4. Estimation of the dynamic protein production and transfer rates during cell cycle divisionin cells grown on glucose. Cells were categorized based on the time between bud appearance (t = 0) and cytokinesis. The data per category was then fitted to the differential equation model for three of the categories (50, 60 or 70 min). Protein production and transfer rates were aligned at cytokinesis (t = 0) for each category (50, 60 and, 70 min). (A) Rate of protein synthesis in the mother cell as a function of time. We could not continuously determine protein synthesis rates in the mother cell during the complete cell cycle, because the data was analysed with two separate differential equation models (one for the period in which the mother cell has a bud and one for the period in which the mother cell does not). (B) Rate of protein transfer to the daughter cell as a function of time. (C) Rate of protein synthesis in the daughter cell as a function of time. (D) The fraction of GFP fluorescence in the daughter cell produced by the mother cell. Protein synthesis and transfer rates are expressed as GFP fluorescence intensity (a.u./min). The estimated degradation rates were k_d^{-1} = 213, 173 and 194 min for the 50, 60 and 70 min datasets.

and peaked in the middle and decreased again until cytokinesis (Figure 4B). The protein production rate of daughter cells was found to increase linearly after bud appearance (Figure 4C). Remarkably, at the time of cytokinesis still roughly 80% of the protein present in the bud appeared to be synthesized by the mother cell (Figure 4D). After cytokinesis, the protein production rate of the mother cell seems to decrease slowly (Figure 4A) causing the mother cell to accumulate protein and increase in size.

A lower rate of protein synthesis appears to reduce the amount of overproduced protein

Above, we found that cells grow in size at a lower rate with replicative age on galactose and pyruvate compared to glucose (Figure 1). We hypothesized that cells would have generally lower protein synthesis rates on these substrates and therefore accumulate less protein after mitosis. To test this, we expressed the fluorescent protein timer in cells growing on galactose and analyzed the data using the differential equation model. While we found similar profiles of protein production and transfer on galactose and glucose (Figure S5), protein synthesis rates were lower on galactose than on glucose. This lower protein synthesis rate leads to a seemingly lower amount of protein overproduction after mitotic exit and thus a lower volume increase per bud on galactose compared to glucose.

Cell size increases in mother cells at a similar rate as in virgin daughter cells

We hypothesized that the cell size increase was a trigger for cell cycle initiation in mother cells (29). In virgin daughter cells, initiation of the cell cycle correlates with cell size growth (30, 31). We therefore wondered whether the cell size increase rate in mother cells prior to bud appearance was similar to the cell size increase rate observed in virgin daughter cells prior to initiation of their first cell division cycle. Here, we found that the cell size increase rates of mother and daughter cells were similar on glucose as well as on pyruvate (Mann-Whitney
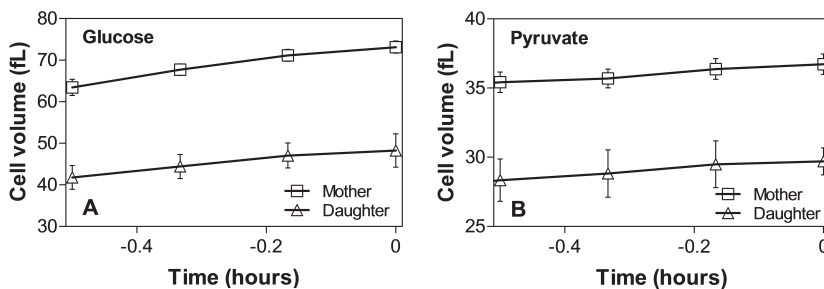

Figure 5. Mother and virgin daughter cells increase in cell size at a similar rate prior to bud appearance on glucose (top) and pyruvate (bottom). n = 50 cells or more. Error bars indicate 95% CI.

U; p = 0.84 for glucose (n = 100 cells) and p = 0.161 for pyruvate (n = 84 cells) Figure 5) suggesting that an increase in cell size may be a requirement for cell cycle progression in both mother and daughter cells.

Discussion

Using our microfluidic setup for long-term microscopic monitoring of single yeast cells, we were able to measure cell size in a highly dynamic manner for extended time periods under stable conditions. We found that the volume of the mother cell increases linearly with age at a rate that depends on substrate. Zooming into single cell cycles, we found that the volume of the mother cell oscillates during the cell cycle with a slight decrease during the first half of the cell cycle after bud appearance and a rapid increase during the second half of the cell cycle until the next bud appears. Further, our study also provides a quantitative estimation of dynamic protein synthesis and transfer rates during the cell cycle. On the basis of these findings, we conclude that the rate of protein synthesis is not adequately down regulated after mitosis causing the mother cell to increase in cell size. The amount of protein that accumulates per division can be modulated by nutritional conditions. The generally lower protein synthesis rates on galactose causes less protein to be overproduced after cytokinesis leading to a lower size increase rate on galactose compared to glucose.

Although we now understand why cells increase in cell size with replicative age, an important question remains; why do cells not achieve homeostasis after mitosis? Until now, no correlation was found between the mother cell size increase (rate) and cell cycle initiation (24, 32). It seems therefore that cell size increase rate in mother cells has no regulatory function. Interestingly, we observed that mother cells increased at a similar rate in cell size as daughter cells prior to the start of cell division suggesting that cell growth may be a requirement for cell cycle initiation in mother cells as well as daughter cells. A coupling between growth potential and cell division in mother cells would enable cells to initiate cell division only under favorable conditions.

Our findings suggest that the rate of cell size increase with replicative age is dependent on the rate of protein synthesis. In literature, cell size, protein synthesis rates and RLS were all shown to be modulated in response to nutrients by the highly conserved target of rapamycin complex 1 (Tor1) (33-36). We therefore hypothesize that Tor1 activity sets the rate of cell size increase with replicative age by regulating ribosome protein synthesis.

Similar to yeast, several types of senescent mammalian cells, *e.g.* human fibroblasts, also have an increased cell size (37-40). Whether these cell size increases in mammalian cells are also caused by repeated rounds of overproduction of protein is unclear (41), especially since the enlarged cell size in mammalian cells appear to occur after cessation of cell division (42, 43). It remains therefore to be seen whether cell size and cell cycle are linked in a similar manner in mammalian cells as in yeast cells (44-47).

Acknowledgment

References

1. Yang J, *et al.* (2011) Cell size and growth rate are major determinants of replicative lifespan. *Cell Cycle* **10**(1): 144-155.

2. Denoth Lippuner A, Julou T & Barral Y (2014) Budding yeast as a model organism to study the effects of age. *FEMS Microbiol Rev* **38**(2): 300-325.

3. Turner JJ, Ewald JC & Skotheim JM (2012) Cell size control in yeast. *Curr Biol* **22**(9): R350-9.

4. Lin SS, Manchester JK & Gordon JI (2001) Enhanced gluconeogenesis and increased energy storage as hallmarks of aging in *Saccharomyces cerevisiae*. *J Biol Chem* **276**(38): 36000-36007.

5. Yiu G, *et al.* (2008) Pathways change in expression during replicative aging in *Saccharomyces cerevisiae*. *J Gerontol A Biol Sci Med Sci* **63**(1): 21-34.

6. Levy SF, Ziv N & Siegal ML (2012) Bet hedging in yeast by heterogeneous, age-correlated expression of a stress protectant. *PLoS Biol* **10**(5): e1001325.

7. Bilinski T, Zadrag-Tecza R & Bartosz G (2012) Hypertrophy hypothesis as an alternative explanation of the phenomenon of replicative aging of yeast. *FEMS Yeast Res* **12**(1): 97-101.

8. Wright J, Dungrawala H, Bright RK & Schneider BL (2013) A growing role for hypertrophy in senescence. *FEMS Yeast Res* **13**(1): 2-6.

9. Kaeberlein M (2012) Hypertrophy and senescence factors in yeast aging. A reply to bilinski *et al.* *FEMS Yeast Res* **12**(3): 269-270.

10. Ganley AR, Breitenbach M, Kennedy BK & Kobayashi T (2012) Yeast hypertrophy: Cause or consequence of aging? reply to bilinski *et al.* *FEMS Yeast Res* **12**(3): 267-268.

11. Moretto F, Sagot I, Daignan-Fornier B & Pinson B (2013) A pharmaco-epistasis strategy reveals a new cell size controlling pathway in yeast. *Mol Syst Biol* **9**: 707.

12. Kaeberlein M, Kirkland KT, Fields S & Kennedy BK (2005) Genes determining yeast replicative life span in a long-lived genetic background. *Mech Ageing Dev* **126**(4): 491-504.

14

13. Mortimer RK & Johnston JR (1959) Life span of individual yeast cells. *Nature* **183**(4677): 1751-1752.

14. Di Talia S, Skotheim JM, Bean JM, Siggia ED & Cross FR (2007) The effects of molecular noise and size control on variability in the budding yeast cell cycle. *Nature* **448**(7156): 947-951.

15. Elliott SG & McLaughlin CS (1978) Rate of macromolecular synthesis through the cell cycle of

the yeast *Saccharomyces cerevisiae*. *Proc Natl Acad Sci U S A* **75**(9): 4384-4388.

16. Godin M, *et al.* (2010) Using buoyant mass to measure the growth of single cells. *Nat Methods* **7**(5): 387-390.

17. Lee SS, Avalos Vizcarra I, Huberts DH, Lee LP & Heinemann M (2012) Whole lifespan microscopic observation of budding yeast aging through a microfluidic dissection platform. *Proc Natl Acad Sci U S A* **109**(13): 4916-4920.

18. Kummel A, *et al.* (2010) Differential glucose repression in common yeast strains in response to HXK2 deletion. *FEMS Yeast Res* **10**(3): 322-332.

19. Khmelinskii A, *et al.* (2012) Tandem fluorescent protein timers for in vivo analysis of protein dynamics. *Nat Biotechnol* **30**(7): 708-714.

20. Gietz RD & Woods RA (2002) Transformation of yeast by lithium acetate/single-stranded carrier DNA/polyethylene glycol method. *Methods Enzymol* **350**: 87-96.

21. Lee SS, Avalos Vizcarra I, Huberts DH, Lee LP & Heinemann M (2012) Whole lifespan microscopic observation of budding yeast aging through a microfluidic dissection platform. *Proc Natl Acad Sci U S A* **109**(13): 4916-4920.

22. Huberts DH, *et al.* (2013) Construction and use of a microfluidic dissection platform for long-term imaging of cellular processes in budding yeast. *Nat Protoc* **8**(6): 1019-1027.

23. Zopf CJ, Quinn K, Zeidman J & Maheshri N (2013) Cell-cycle dependence of transcription dominates noise in gene expression. *PLoS Comput Biol* **9**(7): e1003161.

24. Ferrezuelo F, *et al.* (2012) The critical size is set at a single-cell level by growth rate to attain homeostasis and adaptation. *Nat Commun* **3**: 1012.

25. Waters JC (2009) Accuracy and precision in quantitative fluorescence microscopy. *J Cell Biol* **185**(7): 1135-1148.

26. Alberts B (2002) Molecular biology of the cell, (Garland Science, New York, NY etc.), pp 1463.

27. Costanzo M, *et al.* (2004) CDK activity antagonizes Whi5, an inhibitor of G1/S transcription in yeast. *Cell* **117**(7): 899-913.

28. de Bruin RA, McDonald WH, Kalashnikova TI, Yates J,3rd & Wittenberg C (2004) Cln3 activates G1-specific transcription via phosphorylation of the SBF bound repressor Whi5. *Cell* **117**(7): 887-898.

29. Dirick L, Bohm T & Nasmyth K (1995) Roles and regulation of cln-Cdc28 kinases at the start of the cell cycle of *Saccharomyces cerevisiae*. *EMBO J* **14**(19): 4803-4813.

30. Schneider BL, *et al.* (2004) Growth rate and cell size modulate the synthesis of, and requirement for, G1-phase cyclins at start. *Mol Cell Biol* **24**(24): 10802-10813.

31. Tyers M, Tokiwa G & Futcher B (1993) Comparison of the *Saccharomyces cerevisiae* G1 cyclins: Cln3 may be an upstream activator of Cln1, Cln2 and other cyclins. *EMBO J* **12**(5): 1955-1968.

32. Di Talia S, Skotheim JM, Bean JM, Siggia ED & Cross FR (2007) The effects of molecular noise and size control on variability in the budding yeast cell cycle. *Nature* **448**(7156): 947-951.

33. Stanfel MN, Shamieh LS, Kaeberlein M & Kennedy BK (2009) The TOR pathway comes of age. *Biochim Biophys Acta* **1790**(10): 1067-1074.

34. Blagosklonny MV & Hall MN (2009) Growth and aging: A common molecular mechanism. *Aging (Albany NY)* **1**(4): 357-362.

35. Powers T & Walter P (1999) Regulation of ribosome biogenesis by the rapamycin-sensitive TOR-signaling pathway in *Saccharomyces cerevisiae. Mol Biol Cell* **10**(4): 987-1000.

36. Hands SL, Proud CG & Wyttenbach A (2009) mTOR's role in ageing: Protein synthesis or autophagy? *Aging (Albany NY)* **1**(7): 586-597.

37. Kuilman T, Michaloglou C, Mooi WJ & Peeper DS (2010) The essence of senescence. *Genes Dev* **24**(22): 2463-2479.

38. Adolphe M, *et al.* (1983) Effects of donor's age on growth kinetics of rabbit articular chondrocytes in culture. *Mech Ageing Dev* **23**(2): 191-198.

39. Cooper S (2004) Control and maintenance of mammalian cell size. *BMC Cell Biol* **5**(1): 35.

40. Sherwood SW, Rush D, Ellsworth JL & Schimke RT (1988) Defining cellular senescence in IMR-90 cells: A flow cytometric analysis. *Proc Natl Acad Sci U S A* **85**(23): 9086-9090.

41. Perillo NL, Naeim F, Walford RL & Effros RB (1993) In vitro cellular aging in T-lymphocyte cultures: Analysis of DNA content and cell size. *Exp Cell Res* **207**(1): 131-135.

42. Kennedy BK, Austriaco NR,Jr & Guarente L (1994) Daughter cells of *Saccharomyces cerevisiae* from old mothers display a reduced life span. *J Cell Biol* **127**(6 Pt 2): 1985-1993.

43. Minois N, Frajnt M, Wilson C & Vaupel JW (2005) Advances in measuring lifespan in the yeast *Saccharomyces cerevisiae. Proc Natl Acad Sci U S A* **102**(2): 402-406.

44. Conlon I & Raff M (2003) Differences in the way a mammalian cell and yeast cells coordinate cell growth and cell-cycle progression. *J Biol* **2**(1): 7.

45. Dolznig H, Grebien F, Sauer T, Beug H & Mullner EW (2004) Evidence for a size-sensing mechanism in animal cells. *Nat Cell Biol* **6**(9): 899-905.

46. Fingar DC, Salama S, Tsou C, Harlow E & Blenis J (2002) Mammalian cell size is controlled by mTOR and its downstream targets S6K1 and 4EBP1/eIF4E. *Genes Dev* **16**(12): 1472-1487.

47. Yamamoto K, *et al.* (2014) Largen: A molecular regulator of mammalian cell size control. Mol *Cell* **53**(6): 904-915.

Supplementary Information

Differential equation model

To estimate the dynamic production and transfer rates, a differential model describing the dynamic change of the number of mCherry-sfGFP fusion proteins in the mother and daughter cell was developed. The model included both the number of proteins where only the sfGFP protein has matured, N_{rG}, and the number of proteins where both the sfGFP and the mCherry have matured, N_{RG}. For the mother and daughter, we denoted the number of such fusion proteins by, respectively, N_{rG}^m, N_{RG}^m, N_{rG}^d and N_{RG}^d. We considered a dynamic protein production rate (in both mother and daughter), a transfer of the proteins from mother to daughter, maturation of mCherry and degradation of both proteins.

In times where the mother and daughter are connected, the model then reads

$$\frac{\mathrm{d}N_{rG}^m}{\mathrm{d}t} = P^m(t) - k_m N_{rG}^m(t) - k_d N_{rG}^m(t) - T_{rG}(t)$$

$$\frac{\mathrm{d}N_{RG}^m}{\mathrm{d}t} = k_m N_{rG}^m(t) - k_d N_{RG}^m(t) - T_{RG}(t)$$

$$\frac{\mathrm{d}N_{rG}^d}{\mathrm{d}t} = P^d(t) - k_m N_{rG}^d(t) - k_d N_{rG}^d(t) + T_{rG}(t)$$

$$\frac{\mathrm{d}N_{RG}^d}{\mathrm{d}t} = k_m N_{rG}^d(t) - k_d N_{RG}^d(t) + T_{RG}(t)$$

where k_m is the maturation rate of mCherry and k_d is the degradation rate, which we assume to be equal for both proteins. $P^m(t)$ and $P^d(t)$ are the production rates in the mother and daughter, respectively, and $T_{rG}(t)$ and $T_{RG}(t)$ the transfer rates of the fusion proteins from mother to daughter. We assume that the transfer rates are given by an intrinsic transfer rate, $T(t)$, multiplied by the gradient in concentration between mother and daughter

$$T_{rG}(t) = T(t)\left(c_{rG}^m - c_{rG}^d\right)$$

$$T_{RG}(t) = T(t)\left(c_{RG}^m - c_{RG}^d\right)$$

After the daughter separates from the mother, the corresponding equation system reads

$$\frac{\mathrm{d}N_{rG}^m}{\mathrm{d}t} = P^m(t) - k_m N_{rG}^m(t) - k_d N_{rG}^m(t)$$

$$\frac{\mathrm{d}N_{RG}^m}{\mathrm{d}t} = k_m N_{rG}^m(t) - k_d N_{RG}^m(t)$$

Estimation of production and transfer rates

The model is formulated in terms of the number of fusion proteins, whereas the experiments actually measured the mCherry and sfGFP fluorescences. We assumed that the measured green, G, and red, R, fluorescence intensities are related to the number of fusion proteins according to

$$G = \gamma(N_{rG} + f N_{RG})$$

$$R = \rho N_{RG}$$

where γ and ρ are parameters that relate the fluorescence intensity to the actual number of molecules. These parameters are instrument and setup specific. f measures the amount of energy lost due to Förster Resonance Energy Transfer (FRET). As used here, f is the fraction of energy that is not lost and was set to $f = 0.827$ based on previous measurements (19).

We did not attempt to estimate the actual number of molecules, as it is sufficient for our purposes to have a quantity proportional to the number of molecules. We do need, however, quantities with the same proportionality constant between fluorescence intensity and number of molecules, rather than the two constants γ and ρ above. Rearranging, we have

$$\rho N_{rG} = f\left(\frac{G}{k} - R\right)$$

$$\rho N_{RG} = R$$

where $k = \gamma f / \rho = 1.22$ was measured independently (see next section). Using this expression we then have a quantity proportional to the number of molecules.

The number of molecules was calculated (using the above expression) for each measured cell, and cells which spent the same length of time connected to the daughter cell were averaged over separately. Data-points with fewer than 10 cells contributing to the average were removed. The production, transfer and degradation rates were then determined from a least-square fit of the differential equation model to the averaged data, approximating the derivatives based on the values of nearby points according to

$$\frac{\mathrm{d}f}{\mathrm{d}t} \approx \frac{f(t + \Delta t) - f(t - \Delta t)}{(t + \Delta t) - (t - \Delta t)}.$$

To ensure that the model together with the extracted functions describe the data well, the average cell fluorescence intensities were calculated from the extracted production and transfer rates. The results are shown in Figure S3 and S5.

Determination of mCherry maturation rate and sfGFP/mCherry fluorescence intensity relation

Cells expressing the protein fluorescent timer were exposed to cycloheximide, allowing us to determine mCherry maturation rate and the relation between mCherry and sfGFP fluorescence intensity independently. Cycloheximide promptly halts protein production, so by adding cycloheximide to cells and only measuring cells without daughters, the situation is one where there is neither protein production nor transfer.

After cycloheximide addition, the green fluorescence rapidly decreased and the red fluorescence increased (Figure S6C), consistent with maturation of mCherry and no further production of sfGFP. At longer time-scales (> 200 min), both the green and red fluorescence signals decreased, which we interpreted as degradation of the fluorescent protein timer (Figure S6C).

We fitted the data to a double exponential decay

$$G = C_{Gm}e^{-k_m t} + C_{Gd}e^{-k_{Gd}t}$$

$$R = C_{Rm}e^{-k_m t} + C_{Rd}e^{-k_{Rd}t}$$

where we forced the maturation process, described by k_m, to be the same for both green and red signal, but otherwise left all parameters free. This description fitted the two signals well (Figure S6C). In this way, we determined the mCherry maturation rate $k_m^{-1} = 46.8$ min, being in close agreement to the published maturation time (48).

Using the fit, we also estimated the contribution of degradation kinetics to the signals (Figure S6D). We did this by setting the decay constants, k_{Gd} and k_{Rd}, corresponding to the degradation process(es) to 0. As expected, we found that after maturation both the green and red signal remained constant, with their ratio being 1.22. At this stage, there are only mature fusion proteins present in which both mCherry as well as sfGFP are matured. We determined that the ratio between the green and red signal under these conditions is

$$\frac{\gamma f}{\rho} = 1.22.$$
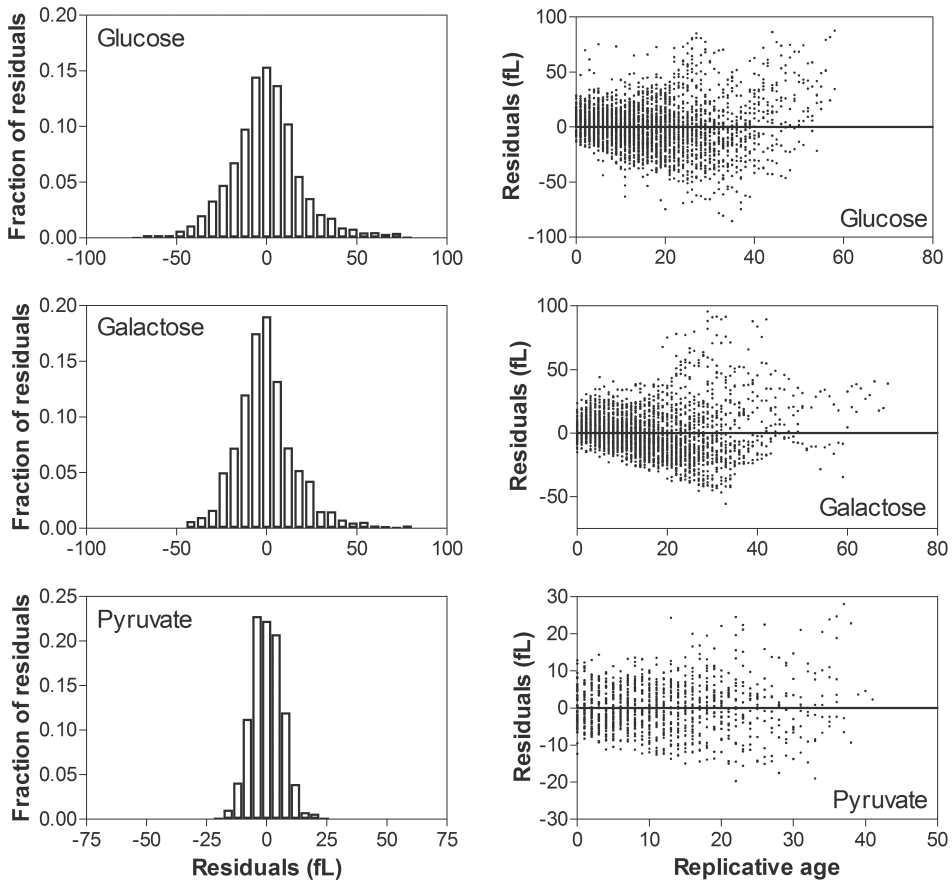
Supplementary Figures

Figure S1. Residuals of fitting cell size versus replicative age data with a linear model. For each carbon source, the residuals are scattered along a horizontal line with replicative age (Spearman's rho; P < 0.01) indicating that the linear model describes the data well.
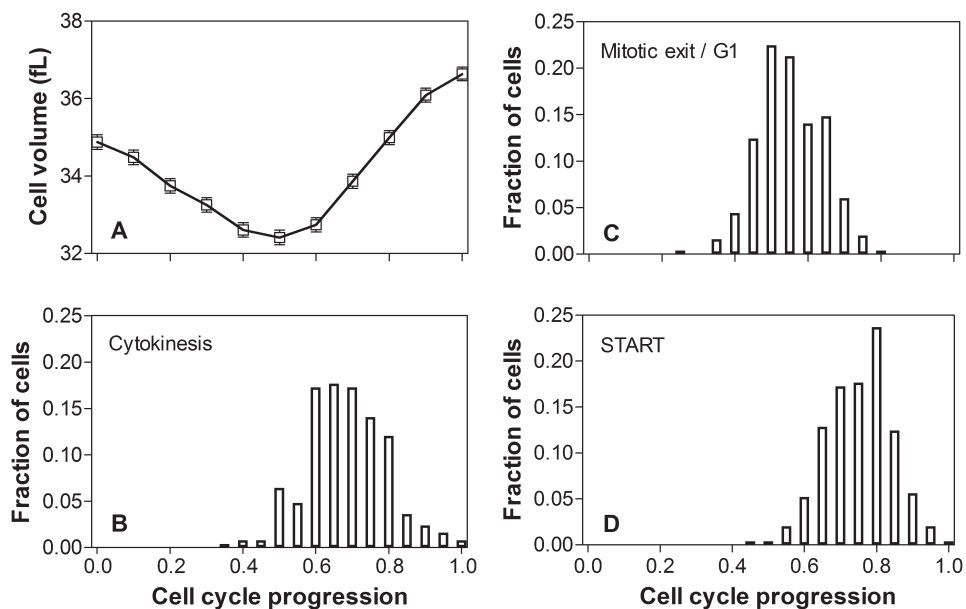
Figure S2. Cell volume increase in mother cells coincides with mitotic exit. Cell cycle duration was normalized using the time between subsequent budding events and defining the time point prior to bud appearance as t = 0. Dotted lines indicate the 95% confidence intervals of the mean. Cells were grown on glucose. (A) Cell volume as a function of cell cycle progression. (B) Histogram representing the distribution of cell cycle progression at which cytokinesis occurred (t = 0.66 ± 0.01 (± SEM)); n = 249 cell divisions). Cell volume starts to increase around t = 0.7, when cytokinesis has only occurred in a minority of the cells suggesting that cytokinesis does not coincide with an increase in cell volume. (C&D) Histogram representing the distribution of cell cycle progression at which Whi5-GFP enters the nucleus referred to as mitotic exit/G1 (C) or exits the nucleus referred to as START (D). On average, Whi5 enters the nucleus at t = 0.53 (SEM < 0.01; n = 249 cell divisions) and exits again at t = 0.73 (SEM < 0.01; n = 249 cell divisions) of cell cycle progression. The cell volume starts to increase at the same time as Whi5 enters the nucleus and continues after Whi5-GFP exits again from the nucleus.
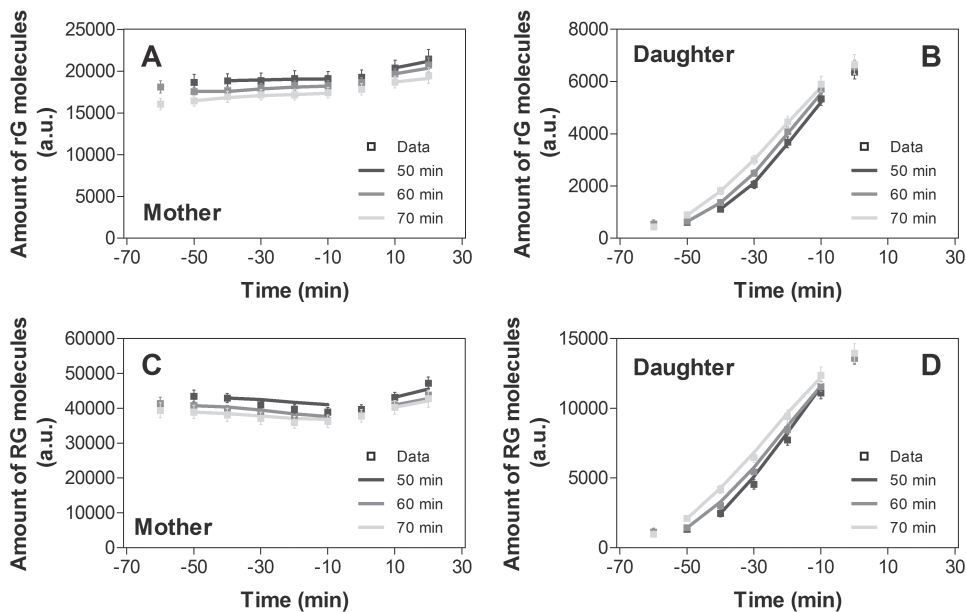
Figure S3. Comparison between experimental data and results obtained from simulations with the differential equation model for cells grown on glucose with 50, 60 or 70 min between bud appearance and cytokinesis. (A&B) Total amount of sfGFP fluorescence intensity per cell derived from tandem fluorescent protein timers in which only sfGFP is mature (rG). We assume that fluorescence intensity directly correlates with the number of rG molecules (N_{rG}) present in mother (A) and daughter (B). (C&D) Total amount of sfGFP fluorescence intensity per cell derived from tandem fluorescent protein timers in which both sfGFP as well as mCherry is mature (RG). After correction for FRET, the fluorescence intensity directly correlates with the number of RG molecules (N_{RG}) present in the mother (C) and daughter (D). Fluorescence intensities were aligned at cytokinesis (t = 0) for each category (50, 60 and, 70 min).
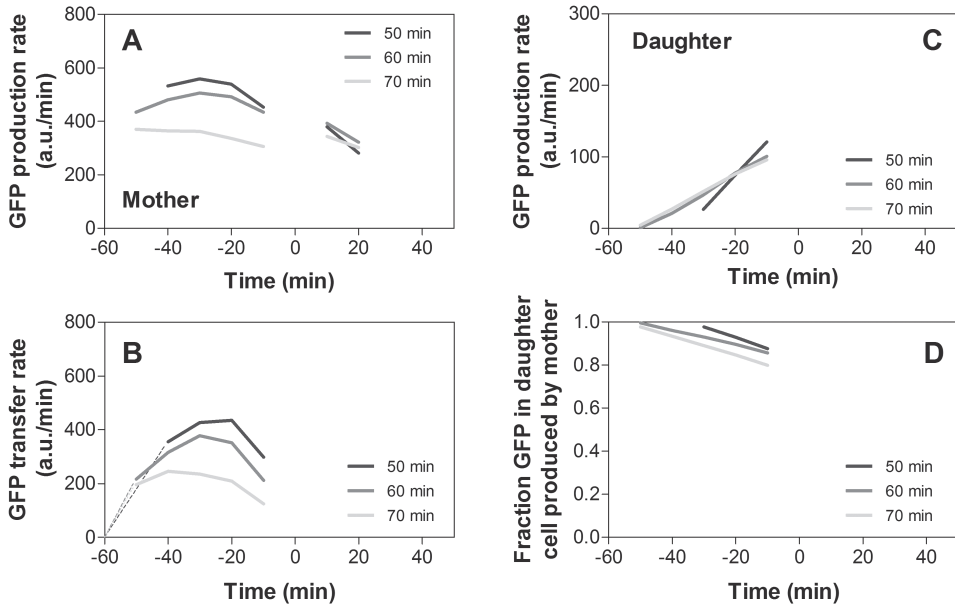
Figure S4. Estimation of the dynamic protein production and transfer rates during cell cycle division in cells grown on galactose. Cells were categorized based on the time between bud appearance (t = 0) and cytokinesis. The data per category was then fitted to the differential equation model for three of the categories (50, 60 or 70 min). Protein production and transfer rates were aligned at cytokinesis (t = 0) for each category (50, 60 and, 70 min). (A) Rate of protein synthesis in the mother cell as a function of time. We could not continuously determine protein synthesis rates in the mother cell during the complete cell cycle, because the data was analyzed with two separate differential equation models (one for the period in which the mother cell has a bud and one for the period in which the mother cell does not). (B) Rate of protein transfer to the daughter cell as a function of time. (C) Rate of protein synthesis in the daughter cell as a function of time. (D) The fraction of GFP fluorescence in the daughter cell produced by the mother cell. Protein synthesis and transfer rates are expressed as GFP fluorescence intensity (a.u./min). The extracted degradation rates were k_d^{-1} = 265, 206 and 279 min for the 50, 60 and 70 min datasets, respectively.
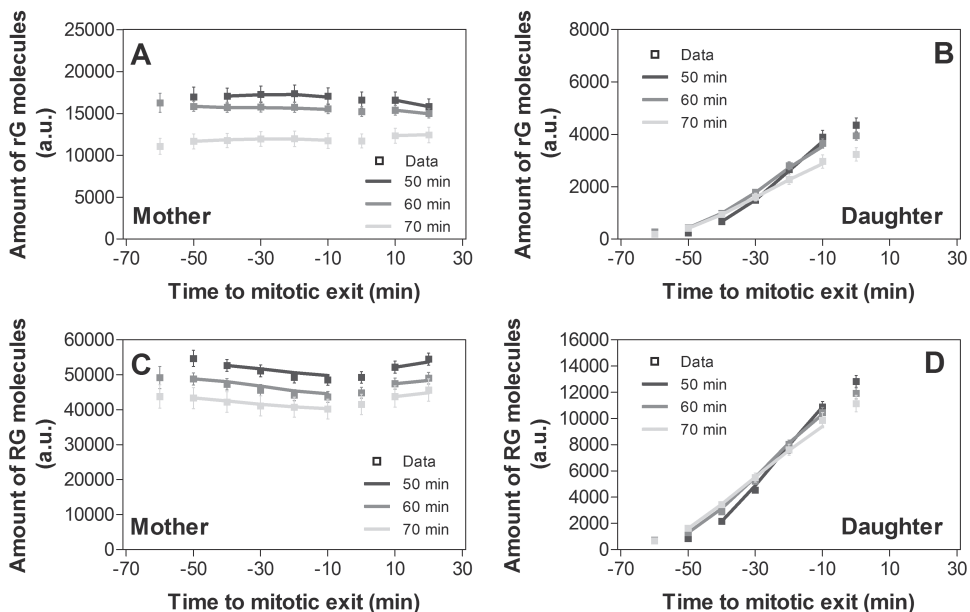
Figure S5. Comparison between experimental data and results obtained from simulations with the differential equation model for cells grown on galactose with 50, 60 or 70 min between bud appearance and cytokinesis. (A&B) Total amount of sfGFP fluorescence intensity per cell derived from tandem fluorescent protein timers in which only sfGFP is mature (rG). We assume that fluorescence intensity directly correlates with the number of rG molecules (N_{rG}) present in either the mother (A) or daughter (B). (C&D) Total amount of sfGFP fluorescence intensity per cell derived from tandem fluorescent protein timers in which both sfGFP as well as mCherry is mature (RG). After correction for FRET, the fluorescence intensity directly correlates with the number of RG molecules (N_{RG}) present in the mother (C) or daughter (D). Fluorescence intensities were aligned at cytokinesis (t = 0) for each category (50, 60 and, 70 min).
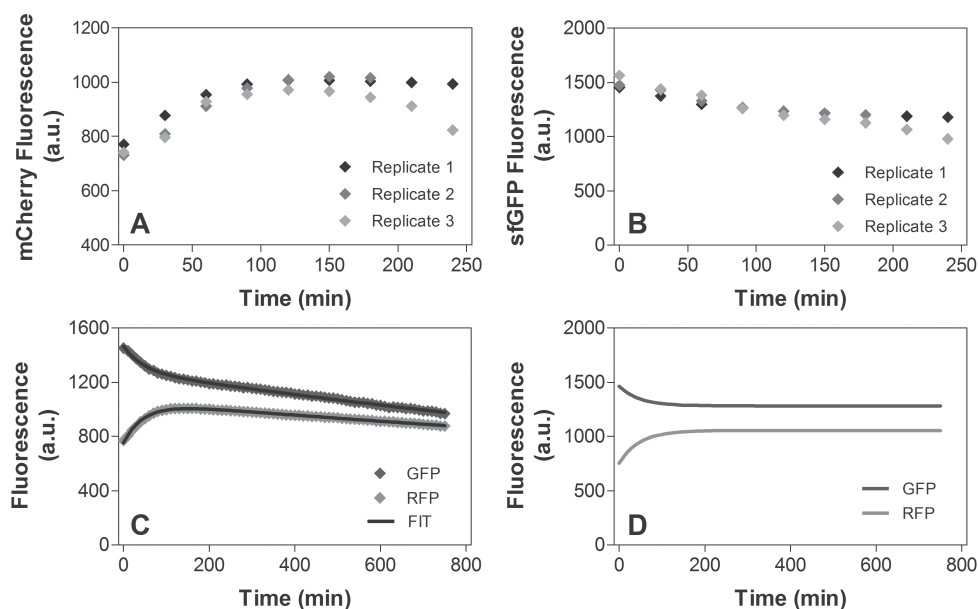
Figure S6. Average mCherry (A) and sfGFP (B) fluorescence intensity after cycloheximide addition (n = 50 cells or more). Experiment was performed with different intervals (twice with 30 min intervals, and once with 10 min intervals). Different imaging intervals do not affect the experimental outcome suggesting that photobleaching did not noticeably affect the outcome of the measurement. At t = 0, cycloheximide (0.05 µg/mL dissolved in YNB medium containing 2% glucose) enters the experimental setup. (C) Determination of maximum ratio between mCherry and sfGFP fluorescence intensity. Average mCherry (red) and GFP (green) fluorescence intensity after cycloheximide addition (n = 162 cells). At t = 0, cycloheximide (0.05 µg/mL dissolved in YNB medium containing 2% glucose) enters the experimental setup. After cycloheximide addition, GFP fluorescence intensity rapidly decreases and mCherry fluorescence increases due to maturation of mCherry and no further production of GFP. After 200 minutes, both the green and red fluorescence signals decrease, which we interpret as degradation of the fluorescent protein timer. We assume that after 200 minutes all mCherry molecules are mature. n = 162 cells (D) After correcting for the linear degradation (see Supplementary Information for details), We determined that the ratio between mCherry and GFP fluorescence intensity was 1.22 in the fully matured fluorescent protein timer.